


Distributed Temperature and Strain Measurements at a Cryogenic Plate-Fin Heat Exchanger Test Rig

Philipp Fritsch^{1,*}, Rainer Hoffmann², Rainer Flüggen², Alexander Woitalka², Patrick Haider¹, Sebastian Rehfeldt¹, and Harald Klein¹

DOI: 10.1002/cite.202100070

 This is an open access article under the terms of the Creative Commons Attribution License, which permits use, distribution and reproduction in any medium, provided the original work is properly cited.

A large cryogenic test rig was built to investigate dynamic operation of plate-fin heat exchangers, which is needed for flexible operation of air separation units. This paper presents results from distributed temperature and strain measurements that were conducted during a dynamic test scenario. Results show that strong temperature gradients appear in all spatial directions of the heat exchangers, resulting in locally varying strains. It is shown that spatially dissolved, dynamic strain measurements are possible using optical fibers. Results from the test rig will help to properly instrument heat exchangers in research and in the field and provide important information for design and operation of plate-fin heat exchangers in dynamic processes.

Keywords: Air separation unit, Distributed measurement, Flexible operation, Optical fiber, Plate-fin heat exchanger

Received: May 19, 2021; *revised:* June 25, 2021; *accepted:* August 06, 2021

1 Introduction

FlexASU is a sub-project of the Kopernikus project SynEnergie, which aims to enable air separation units (ASUs) for demand side management [1, 2] in terms of energy supply. The ability to operate air separation and other energy-intensive industrial processes more flexibly, and hence vary the power demand is attracting growing interest because the higher share of renewable energy sources is leading to an increasingly volatile energy market [3]. For ASUs, the resulting higher number of load changes, shutdowns and restarts can lead to additional cyclic stresses on the equipment, which reduces the expected lifetime [4]. The main heat exchanger is part of an ASU's core equipment and its design is challenging even for conventional ASUs [5]. In an FlexASU this equipment is particularly affected by transient operation conditions due to the resulting temperature changes. Thus, it is important to not only search for the price and energy optimum of operation, but also to take stress on equipment into account when it comes to a flexibly operated ASU. Hence, a detailed examination of transient operation conditions using experimental and simulation methods is required. A large test rig has been put into operation [6, 7] for experimental investigation of aluminum plate-fin heat exchangers (PFHEs), which are commonly applied as main heat exchangers of ASUs [8]. In the test rig, a highly repetitive, intentionally harmful test scenario is conducted to provoke fatigue damage from the resultant cyclic stresses on the PFHE. The fatigue life prediction for

heat exchangers also played a role in [9] for steel PFHEs and in [10] and [11] for fin structures under cryogenic conditions. Nevertheless, the approach of conducting fatigue tests using process streams at different temperatures to induce cyclic stresses in the heat exchangers (as in [12]) accounts for additional influence factors compared to solely applying mechanical force on test bodies, such as in, e.g., [9, 11]. The approach is chosen due to the complex and multidimensional temperature gradients and resulting forces that occur in the dynamic operation of heat exchangers. During the cyclic operation of the test rig, the goal is to gain extensive knowledge of the behavior of PFHEs under dynamic operation. Hence, the repetitive transient cool-downs and warmups are recorded explicitly in terms of temperature and strain. The recorded data is essential for improving and validating a three-dimensional thermo-fluid simulation model [13] and computational lifetime estimation tools [14]. This paper builds on foregoing work con-

¹Philipp Fritsch, Patrick Haider, Dr. Sebastian Rehfeldt, Prof. Dr. Harald Klein
philipp.fritsch@tum.de

Technical University of Munich, Department of Mechanical Engineering, Institute of Plant and Process Technology, Boltzmannstraße 15, 85748 Garching, Germany.

²Dr. Rainer Hoffmann, Rainer Flüggen, Alexander Woitalka
Linde GmbH, Linde Engineering, Dr.-Carl-von-Linde-Straße 6–14, 82049 Pullach, Germany.

cerning the expected lifetime and fatigue in PFHEs at Linde Engineering, including experiments using smaller PFHE specimens [12] and simulation tools [14–16]. After the test rig and applied measurement methods have been described in [7], this paper provides results from temperature and strain measurements of the highly dynamic test scenario. Since several, partly redundant measurement methods are deployed in the test rig, the various methods are compared, and advantages and drawbacks discussed.

2 Materials and Methods

All measurements in this work have been conducted at the cryogenic PFHE test rig, which was presented in [7]. The test rig is operated at similar temperature level as ASUs in the field and all cryogenic plant components are installed in a perlite-filled coldbox. In the test rig, two aluminum PFHE test specimens undergo a highly repetitive series of cool-downs and warmups in a cryogenic temperature range, which are induced by the alternate supply of cold and warm gaseous nitrogen streams. Liquid nitrogen is used as a coolant (see [7] for more details). The sequence of one cool-down and one warmup of equal duration is defined as a cycle, which lasts about 15 min. Up to now, more than 1000 test cycles have been conducted at each of the two PFHE test specimens.

The two PFHE test specimens that are installed on the test rig exhibit dimensions of approx. $1.5\text{ m} \times 1.5\text{ m} \times 0.5\text{ m}$ (length, stacking height and width) and weigh around 1.5 t. The PFHEs are manufactured and brazed analogously to ASU heat exchangers and display the same design elements (see [7]). The three spatial directions of the PFHE test specimens are defined as the length, stacking height and width of the heat exchanger (Fig. 1).

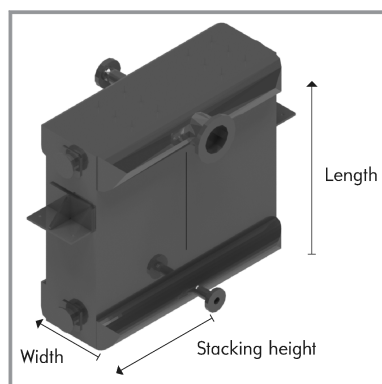


Figure 1. Nomenclature spatial directions PFHE test specimen.

In the description of the results, the position at the PFHE is specified using normalized parameters, which are obtained by dividing the spatial position by the total PFHE length, stacking height or width, respectively. Also, the relative cycle time is used, which is the elapsed time since the start of the cycle divided by duration of one complete cycle.

Besides conventional measurement equipment used for process control, the PFHEs are equipped with scientific temperature and strain instrumentation using advanced measurement methods (cf. [7]). For example, distributed measurements using Rayleigh scattering and fiber Bragg gratings (FBG) in optical fibers are applied. These methods have been known for decades now [17, 18] and offer different advantages. FBG fibers constitute a very reliable, mature technology, and are straightforward in terms of application and data processing. However, this measurement method is not really distributed since measurements are only possible at foreseen sensor positions that are limited by the number of gratings in the fibers. Due to the grating process, FBG fibers are also more expensive. Conversely, measurements using Rayleigh backscattering can be taken with low-cost standard single-mode optical fibers [19], but data processing is more elaborate for this method. At the test rig 14 Rayleigh fibers with a length up to 20 m are applied, allowing temperature measurements between $-196\text{ }^{\circ}\text{C}$ and $50\text{ }^{\circ}\text{C}$ with an accuracy of $3\text{ }^{\circ}\text{C}$ at intervals of a few mm along the fibers [7]. Distributed temperature measurements using optical fibers have been successfully applied in numerous different fields such as long-distance environmental monitoring [20] and nuclear power plants [21]. Also, fiber optical sensors have been used under cryogenic conditions [19], especially in the area of superconducting technology (e.g., [22]). Reviews of distributed temperature-sensing technology and applications can be found in [20, 23, 24]. At Linde, fiber-based temperature measurements have already been applied coil-wound heat exchangers [25].

Methods using optical fibers are compared to well-established measurement methods like Pt100 temperature sensors and position sensors. The advantages and drawbacks of the different measurement methods will be addressed in the results section. A more detailed description of the test rig, test scenario, PFHE test specimens and measurement methods can be found in [6] and [7].

3 Results and Discussion

While in total, over 1000 cycles per PFHE were completed on the test rig, the results in the following are presented just for one or a small number of these cycles. The cycles themselves are highly repetitive, hence measurements from different cycles can be used together for evaluation without loss of information.

3.1 Comparison of Different Temperature Measurement Methods

At the surface of the PFHE test specimen, the location of two Pt100 temperature sensors coincides with the route of two Rayleigh optical fibers in two points at a relative stacking height of 0.5 at two different relative lengths. Hence, the

results of these two measurement methods can be compared for one exemplary cycle (see Fig. 2). The two measurement points have a distance of 15 cm.

The overall temperature range is slightly above and below room temperature, since measurements at a relative length of the PFHE of 0.27 and 0.37 are shown here. At the cold end of the PFHE, lower temperatures prevail. The temperatures of the two different measurement systems at the surface show good agreement, especially concerning the dynamic of the test scenario. There is no sign of delay in the comparison of both methods. This is a pleasant verification for the advanced optical fiber measurement system since Pt100s are a very reliable and well-established temperature measurement device. Nevertheless, there are some deviations especially in the higher temperature range ($T > 40\text{ }^{\circ}\text{C}$). The main reason for this is the difficulty in installing the sensors on the surface of the PFHEs such that thermal contact is ensured. The fibers run through thin metal capillaries, which were glued to the surface using aluminum tape. The Pt100s were glued onto the surface using a special adhesive. The thermal contact can be affected by the clearance between PFHE and the sensors and the thickness of the adhesive.

While in Fig. 2 only one location of the respective fiber is depicted, Rayleigh-based fiber temperature sensing is capable of measuring temperatures along the complete fiber at intervals of just a few mm. Another temperature-sensing method using optical fibers that is applied on the test rig are FBGs [7]. This method uses specially prepared fibers and offers measurements at several discrete points along a fiber. In the case of the test rig, each fiber includes 13 sensors a few cm apart. In Fig. 3, the results of three FBG fibers inside the PFHE are compared to the three parallel Rayleigh fibers at the end of the cooldown phase (relative cycle time: 0.5). The fibers are distributed over the width of the PFHE (relative width: 0.17, 0.5 and 0.83) at a relative stacking height of 0.5.

The two measurement methods display good agreement, especially in the cold section of the heat exchanger. Since FBG fibers offer some benefits in data recording and processing, especially compared to Rayleigh-based fibers, it is a promising tool for application in equipment in the field. However, FBG measurements are not truly distributed and discrete sensor points must be chosen in advance leading to a loss of information compared to the Rayleigh optical fibers. Therefore, the measurement based on Rayleigh fibers is more suitable for application in research, where effort and handling are less important.

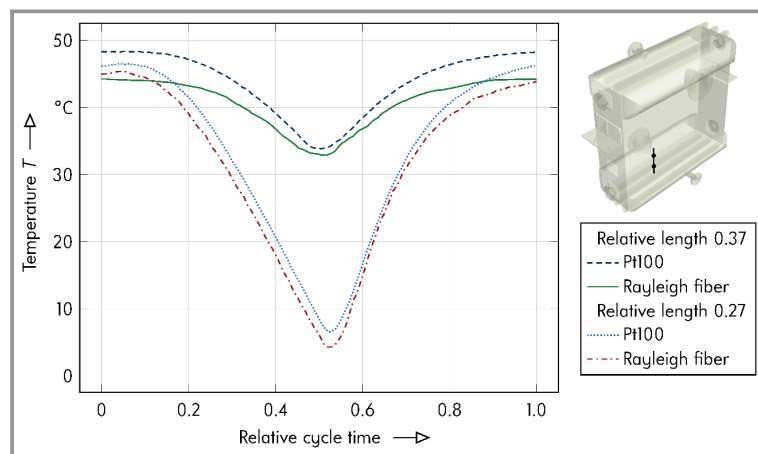


Figure 2. Comparison of Pt100 and fiber-optical surface temperature measurements.

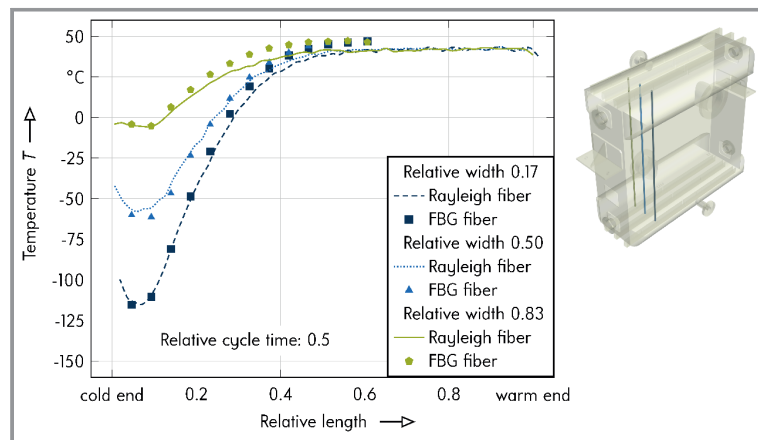


Figure 3. Comparison of FBG and Rayleigh fiber-optical temperature measurement.

In Fig. 2 and 3, temperature measurements at the surface and inside the PFHE are presented, respectively. Temperature sensors at the surface are easier to install and can be retrofitted to existing equipment. Therefore, it would be advantageous if these sensors were sufficient to observe all occurring effects. Fig. 4 shows the temperatures of one test cycle measured at two points within two Rayleigh optical fibers within (relative width: 0.17) and on the surface (relative width: 0) of the PFHE and one conventional Pt100 at the surface, all at the same relative stacking height (0.5) and length (0.37) of the heat exchanger.

While the two measurement methods on the surface show the known behavior and close agreement with each other, the inside fiber differs in its results. It shows a higher amplitude of temperature and different dynamic behavior. As seen in Fig. 4 surface measurements are subject to a delay, and temperature changes within the heat exchanger are noted at the surface shortly after. Contrarily, a change in

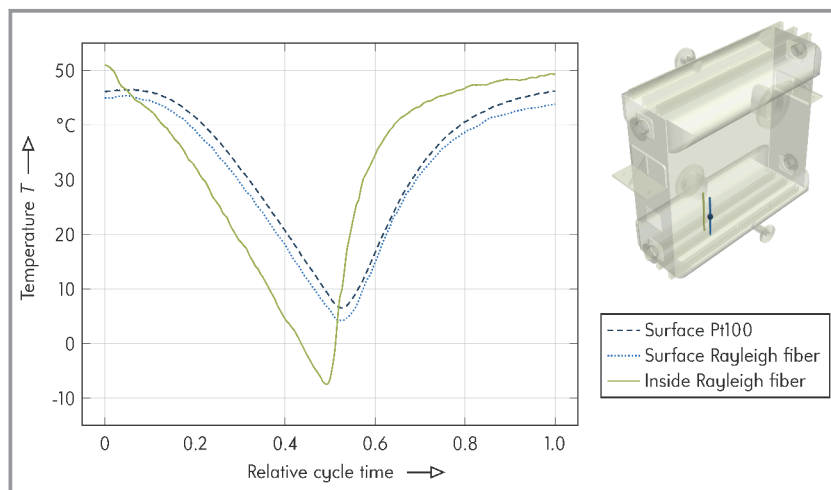


Figure 4. Comparison of dynamic temperature measurements on the surface and within the PFHE.

temperature in the gas flow is directly discernible using the inside fiber. This can be explained with the inside measurements being in closer contact with the gas flow and less influenced by thermal mass effects. Differently, surface measurements are separated from the gas flow by solid metal mainly by sidebars. This metal supports thermal inertia and slows down the discernible temperature change. Hence, the measured amplitude is also smaller at the surface. Consequently, surface measurements are less suitable if the temperatures inside the PFHE are required, especially in the present, highly dynamic scenario. Therefore, only temperature measurements from inside the PFHE are presented in the following.

3.2 Temperature Distribution within the PFHE

Within a heat exchanger, a temperature gradient from the inlet to the outlet of the process streams is implied by the working principle of this equipment. Usually, this gradient is much higher than the gradients in the other two spatial directions. Hence, depicting and modeling a heat exchanger is often simplified in a one-dimensional thermal manner. While this approximation is usually justified for operation of the heat exchanger at design operating point, this may not be the case for atypical operation modes occurring during load changes, shutdowns or restarts of the plant. The test scenario is especially atypical, since the fast temperature changes are induced by the alternating supply of warm and cold gas streams, in contrast to countercurrent flow in PFHEs in the field.

Fig. 5 shows the temperatures measured by three optical fiber segments distributed over the stacking height all at a relative PFHE width of 0.17 of the PFHE at different times of the cycle. The temperature at the warm end of the heat exchanger is intentionally unaffected throughout the cycle.

The cold end of the PFHE is cooled from around 0°C at the beginning of the cycle to around -125°C at the end of the cooldown (relative cycle time: 0.5). The local minimum in the temperature profiles can be attributed to the different heat transfer inlets along the pathway of the process stream (cf. [7]). Beside the distinct temperature gradient along the main flow direction, a comparably small difference of approx. 30°C builds up between the three fibers along the stacking height of the PFHE. The fiber closest to the cold gas inlet shows the lowest temperatures, while the ones further from the inlet display higher temperatures. Hence, the temperature is not equally distributed over the stacking height of the PFHE but shows an additional gradient due to the interaction inertia of

thermal mass and distribution of the cold gas over the passages. This effect is even more pronounced looking at the third spatial direction, the passage width of the heat exchanger.

In Fig. 6 the temperatures of three optical fibers distributed over the width of the PFHE all at a relative stacking height of 0.25 are shown. In this direction the temperature difference between fibers at a relative PFHE width of 0.17 and 0.83 sums up to approx. 110°C, which is in the same order of magnitude as the temperature gradient in the main flow direction of the heat exchanger. While the fiber closest to the gas inlet exhibits rapid cooling, the fiber furthest from the inlet in a widthwise direction is just beginning to react at the end of the cooldown.

As a result of the measurements, simplifying assumptions leading to a common wall 1D thermal simulation approach are not permissible, at least for the test scenario [2]. Strong 3D effects may also occur in PFHEs in the field, especially in atypical operation modes. It is important to include these effects by a 3D finite-element analysis when it comes to lifetime estimation tools. The lifetime strongly depends on the occurring temperature gradients and thermal stress. Hence, detailed observation of the heat exchangers in operation using distributed temperature sensing inside the PFHE is appropriate. Additionally, proper design and lifetime estimation using 3D modeling tools is required. The considerations based on the results of the test rig in combination with simulation results have led to the development of a 3D computational fluid dynamics model [13], which can be used for that purpose.

3.3 Strain Measurements

As a result of the 3D temperature distribution within the heat exchangers, different areas of the heat exchanger show

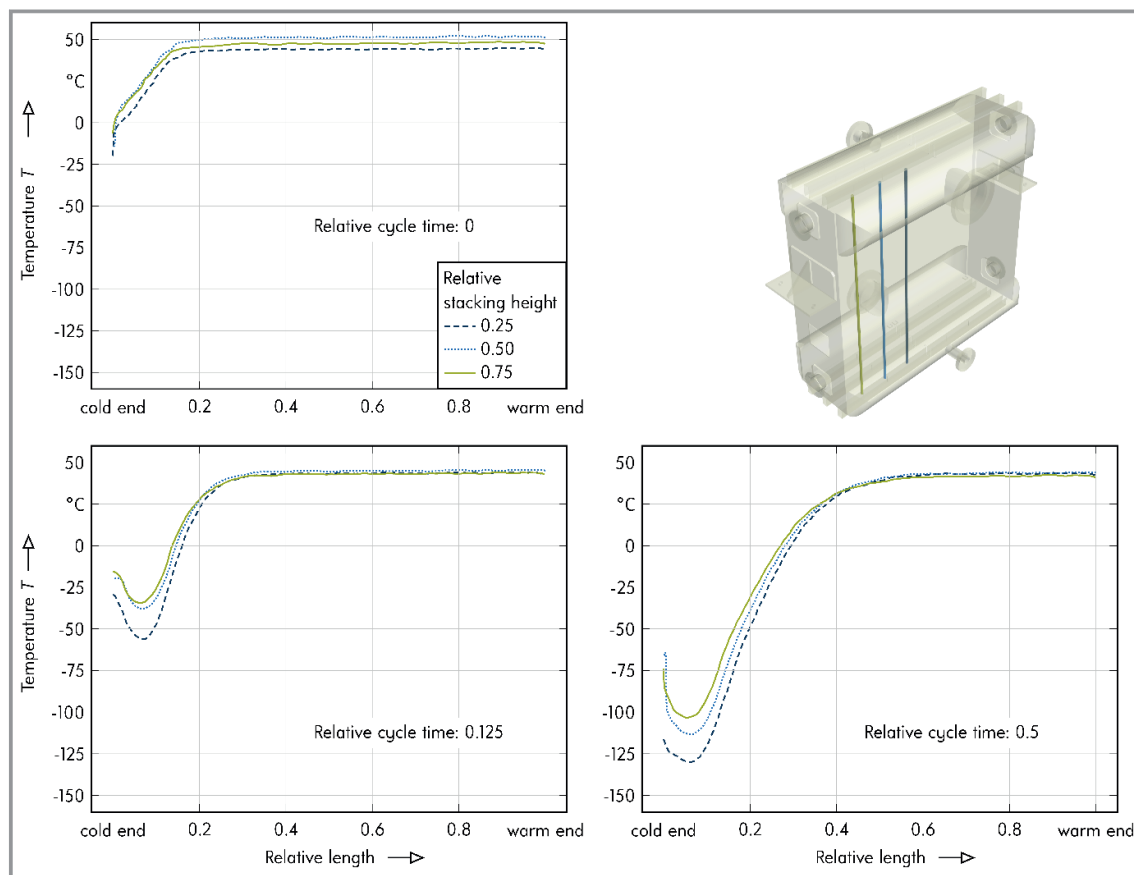


Figure 5. Temperature distribution over PFHE stacking height.

different thermal expansion and shrinking. In Fig.7 the expansion in different spatial directions compared to the beginning of the cycle is shown using four position sensors at different edges of the PFHE. The sensors record the position change of one end of a pole, while the other end is fixed at the PFHE and therefore the integral expansion or shrinking along this pole.

As expected, the position sensors at both front ends of the heat exchanger display close agreement over time. This is due to the symmetrical behavior of the PFHE along the gas inlets. In the first half of the cycle, cold gas enters the PFHE and cools it down starting from the gas inlet. Hence, the sensors show shrinking. In the second half, the PFHE is heated up again and expands to the initial level. While the sensors in the front and back run in a direction whereby the warm end is not experiencing cooling, the sensor over the stacking height records cooling over the whole length. For this reason, the recorded shrinking is around six times larger compared to the position sensors running over the front length. The shrinking measured over the length in the rear part of the PFHE is significantly smaller compared to the position sensors in the front, even though they are installed in the same spatial direction. The shrinking can be directly linked to the temperature difference over the cycle and thus

is also smaller in the rear part of the PFHE (for temperature see Fig. 6). The signal even appears to show a small expansion in the rear part of the PFHE, but this can be attributed to a delay in temperature progression in the rear part of the PFHE due to thermal inertia of the metal. Hence, the rear part of the PFHE does not show the highest expansion in the beginning of the cycle (relative cycle time: 0). The expansion along the PFHE width was also measured but does not provide new insights and is therefore not shown here.

Another method to conduct strain measurement at the test rig are Rayleigh optical fibers. Using this method, the distributed strain, which is the local strain along the fiber, is accessible. The required setup to measure distributed strains using Rayleigh fibers is described in [7]. In Fig. 8 the normalized local strain over one cycle, measured by a fiber segment at the surface along the PFHE length, is depicted. The fiber does not cover the whole length of the PFHE since its installation path is interfered by the suspension of the PFHE within the test rig. The normalized strain was obtained by dividing the measured strain values by a reference strain.

The fiber segment runs along the main flow direction of the heat exchanger from the cold end to a relative PFHE

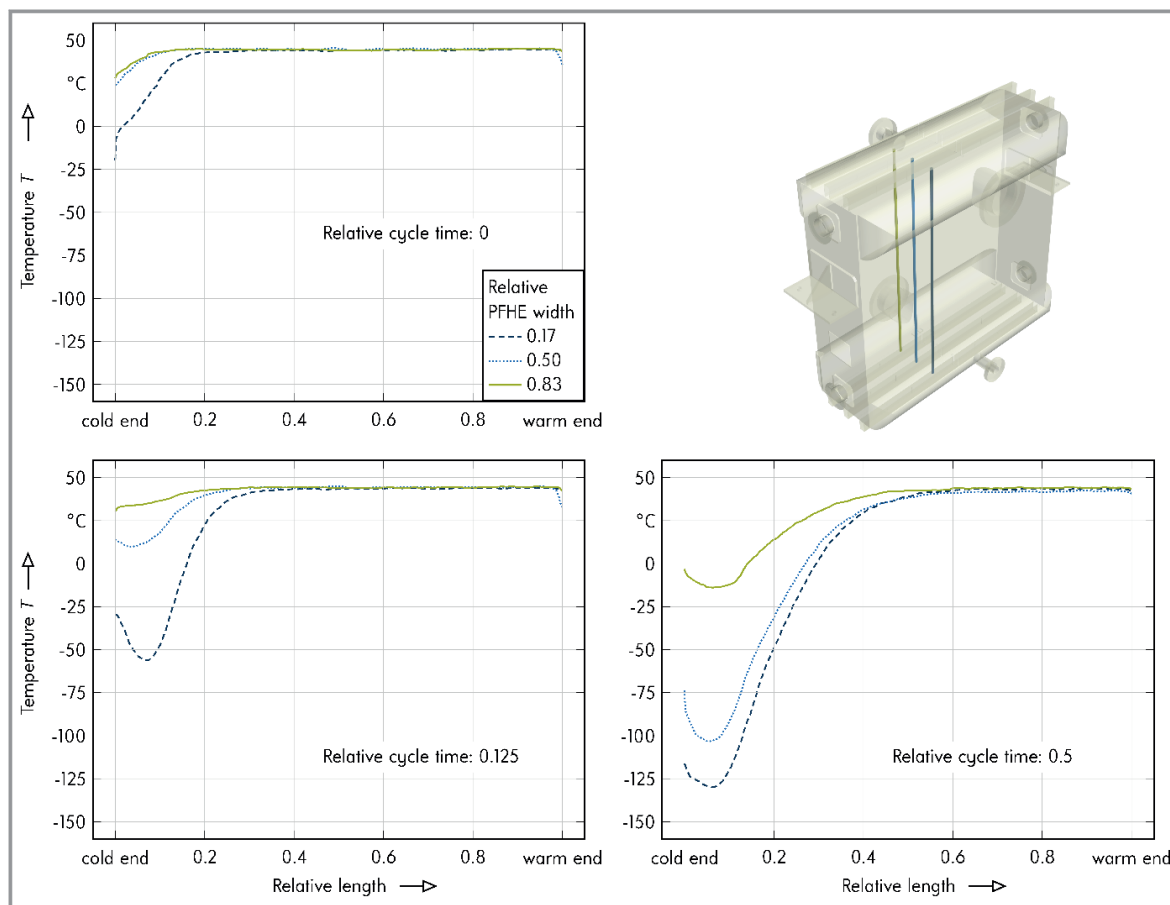


Figure 6. Temperature distribution over PFHE width.

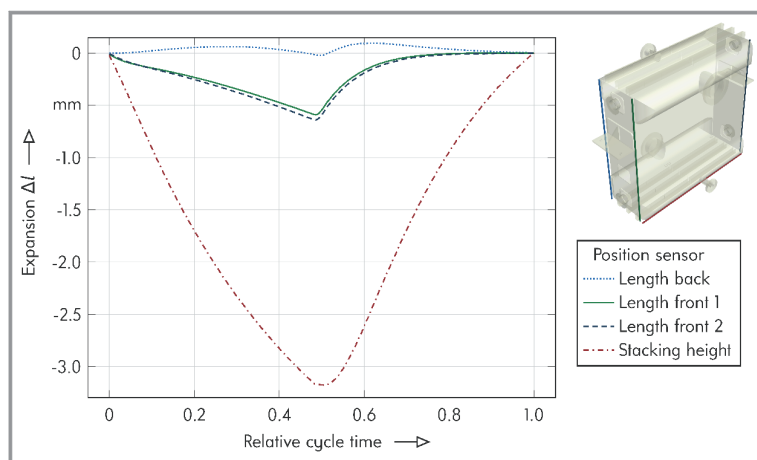


Figure 7. Thermal shrinking and expansion of the PFHE measured by position sensors.

length of approx. 0.6. At the upper part of the of the heat exchanger (relative fiber length > 0.6), a temperature of approx. $45\text{ }^{\circ}\text{C}$ prevails throughout the cycle. Since the temperature is above room temperature, the metal is expanded compared to that state, and positive strains are measured.

The bottom part of the heat exchanger shrinks due to the cold gas supply and negative strain values are measured climaxing at the end of the cooldown process (relative cycle time: 0.5). Furthermore, since the temperature difference to room temperature is larger at the cold end, the negative strain values are higher than the positive ones in the warm end. Additionally, it is discernible that the cooling propagates from the cold end of the PFHE in the first half of the cycle and withdraws again in the second half of the cycle.

Using more than one fiber, an overall view of the heat exchanger can be assembled, and 3D dynamic strain measurements are possible.

Since this measurement method is relatively new and advanced, it is necessary to check the results using a simpler measurement method.

This can be done by calculating the integral strain, which is obtained by integrating the measured local strains along the fiber and comparing this overall expansion with the results of a position sensors. The position sensors have a measuring range of 0 to 10 mm with an accuracy of 0.1%. In Fig. 9 the same fiber segment as in Fig. 8 is

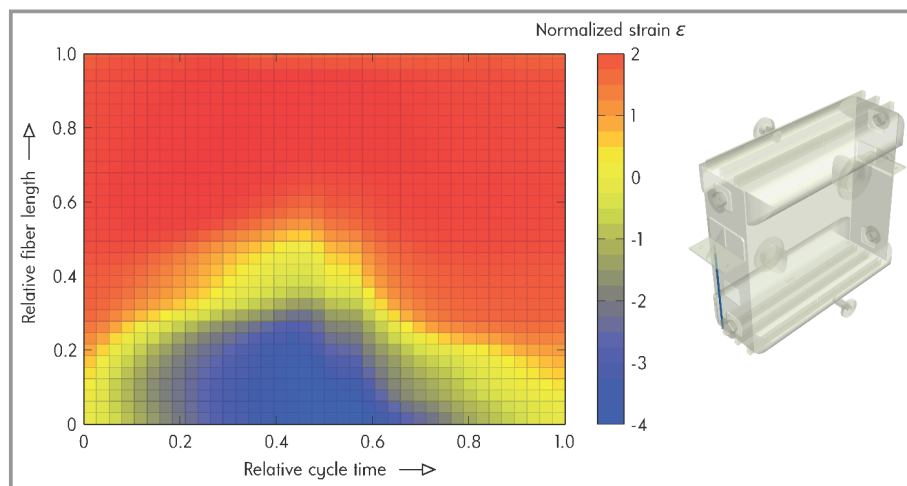


Figure 8. Distributed strain measurement using optical fiber.

compared to the signal of a position sensor, which runs parallel to that fiber.

The position sensor shows a repetitive signal since several cycles are shown here. Starting from a relative cycle time of around 2.4, the parallel running fiber was also measured. The fiber does not cover the whole length of the PFHE, but since the warm end of the heat exchanger preserves the same temperature throughout the cycle, it can be neglected in terms of the overall expansion. The calculated integral strain of the fiber shows good agreement with the position sensor. In particular, the dynamic captured is similar in both methods. The overall amplitude is slightly higher for the fiber method. However, with regard to the uncertain measurement accuracy of the fiber strain measurement, the two methods show sufficient agreement.

As a third method to conduct strain measurement at the test rig, strain gauges are installed at important areas of the PFHE. Results of this method are not presented in this

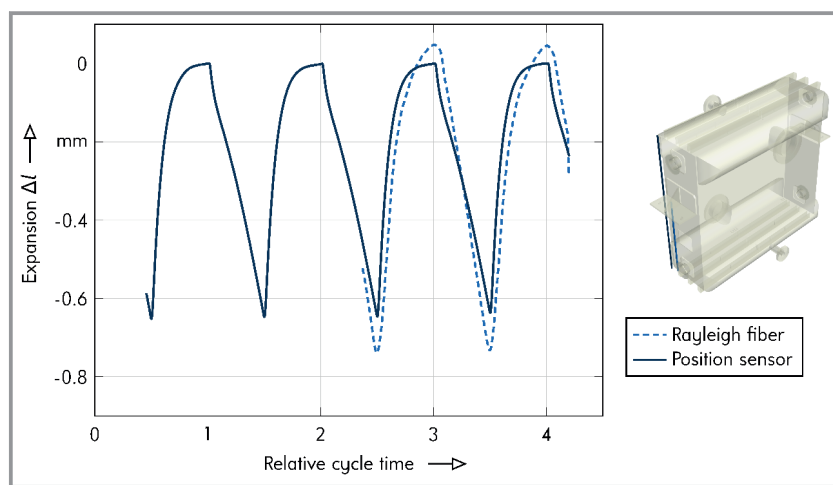


Figure 9. Integral strain of fiber compared to expansion recorded by position sensor.

paper, but an example for strain gauge measurements of the test scenario can be found in [7].

4 Conclusion

Several different temperature and strain measurement methods were applied to examine a highly dynamic test scenario on a cryogenic PFHE test rig.

Rayleigh-based fiber temperature measurements were qualified using Pt100 sensors at the same locations. Optical fiber temperature measurements using FBGs were also applied on the test rig and exhibited close agreement with the Rayleigh based measure-

ments. FBG-based measurements entail some simplifications in application and are a promising method to be installed on equipment in the field. However, compared to Rayleigh optical fiber measurements, the number of sensors is limited, and measurement is hence not really distributed.

Rayleigh optical fibers were used to collect distributed, dynamic temperature data. Concerning the location of the fibers, measurements inside the PFHE were more suitable to capture dynamic temperature effects in the test scenario. Surface measurements showed a delay compared to measurements inside the PFHE. Using distributed temperature measurement methods, a strong 3D temperature distribution was recorded for the test scenario. This shows that a common wall 1D thermal-simulation approach, where only the temperature gradient in the main flow direction is considered, is not sufficient, especially for PFHEs in atypical operation modes. Lifetime estimation tools need information about the 3D temperature distribution since temperature gradients are a main reason for thermal stress.

Position sensor measurements have shown that the PFHE is subject to a different overall expansion depending on the location. Areas close to the cold gas inlet are cooled to lower temperatures and therefore display higher thermal shrinking. Hence, PFHEs under dynamic operation need to be designed properly using 3D transient thermal simulation tools (e.g., [13]), which capture local thermal mass effects and directional heat conduction to predict realistic fatigue behavior.

While position sensors only record the overall strain, Rayleigh optical fiber measurements are a suitable measurement method to obtain distributed strain as well as the integral strain along the fiber. By combining signals from several fibers,

dynamic 3D distributed strain measurements are possible for the use case of a cryogenic PFHE. However, this method is associated with considerable effort in installation and analysis, since additional fibers have to be installed in the same position, which solely measure the temperature-induced frequency shift in the fiber, and their signal must be subtracted in order to isolate the distributed strain of the underlying metal [7].

This paper presents various methods that can be applied in research to monitor dynamic 3D experiments not only in PFHEs, but also in other applications where transient temperatures and strains are of interest. However, some of the methods may be too elaborate for monitoring the everyday operation of equipment in the field.

The results of the test rig are used to validate 3D dynamic PFHE simulation and computational lifetime estimation tools. This will help to properly design PFHE for their application in flexibly operated air separation units and other processes.

The authors gratefully acknowledge the financial support of the Kopernikus project “SynErgie” and “SynErgie2” by the German Federal Ministry of Education and Research (BMBWF, FKZ 03SFK3E1 and FKZ 03SFK3E1-2) and the project supervision by the project management organization Projektträger Jülich (PtJ). Open access funding enabled and organized by Projekt DEAL.

Symbols used

Δl	[mm]	Expansion
T	[°C]	Temperature

Greek letters

ε	[-]	Normalized strain
---------------	-----	-------------------

Abbreviations

ASU	Air separation unit
FBG	Fiber Bragg grating
PFHE	Plate-fin heat exchanger

References

- A. Sauer, E. Abele, H. U. Buhl, *Energieflexibilität in der deutschen Industrie: Ergebnisse aus dem Kopernikus-Projekt – Synchronisierte und energieadaptive Produktionstechnik zur flexiblen Ausrichtung von Industrieprozessen auf eine fluktuierende Energieversorgung (SynErgie)*, Fraunhofer Verlag, Stuttgart **2019**.
- H. Klein, P. Fritsch, P. Haider, R. Kender, F. Rößler, S. Rehfeldt, P. Freko, R. Hoffmann, I. Thomas, B. Wunderlich, *Chem. Ing. Tech.* **2020**, *92* (12), 1921–1940. DOI: <https://doi.org/10.1002/cite.202000054>
- Q. Zhang, I. E. Grossmann, *Altern. Energy Sources Technol.* **2016**, *78*, 383–414. DOI: https://doi.org/10.1007/978-3-319-28752-2_14
- A. Obermeier, C. Windmeier, E. Esche, J.-U. Repke, *Chem. Eng. Sci.* **2019**, *195*, 904–920. DOI: <https://doi.org/10.1016/j.ces.2018.10.036>
- J. Xu, X. Chen, S. Zhang, Q. Chen, H. Gou, J. Tan, *Appl. Therm. Eng.* **2017**, *113*, 774–790. DOI: <https://doi.org/10.1016/j.applthermaleng.2016.10.177>
- P. Haider, P. Freko, S. Lochner, T. Reiter, S. Rehfeldt, H. Klein, *Chem. Eng. Res. Des.* **2019**, *147*, 90–97. DOI: <https://doi.org/10.1016/j.cherd.2019.04.025>
- P. Fritsch, R. Hoffmann, R. Flüggen, P. Haider, S. Rehfeldt, H. Klein, *Chem. Ing. Tech.* **2021**, *93* (8), 1230–1237. DOI: <https://doi.org/10.1002/cite.202000253>
- H. Hausen, H. Linde, *Tiefenperaturtechnik: Erzeugung sehr tiefer Temperaturen, Gasverflüssigung und Zerlegung von Gasgemischen*, Springer, Berlin **1985**.
- W. Jiang, J. M. Gong, S. T. Tu, *Mater. Des.* **2011**, *32* (10), 4936–4942.
- K. Li, J. Wen, H. Yang, S. Wang, Y. Li, *Int. J. Therm. Sci.* **2019**, *145*, 106013.
- M. H. Saggi, N. A. Sheikh, U. M. Niazi, M. Irfan, A. Glowacz, *Energies* **2020**, *13* (9), 2175. DOI: <https://doi.org/10.3390/en13092175>
- R. Hölzl, R. Flüggen, in *Proc. of the ASME 2013 Pressure Vessels and Piping Conference 2013*, American Society of Mechanical Engineers, New York **2013**, V003T03A093. DOI: <https://doi.org/10.1115/PVP2013-97915>
- P. Haider, P. Freko, T. Acher, S. Rehfeldt, H. Klein, *Appl. Therm. Eng.* **2020**, *180*, 115791. DOI: <https://doi.org/10.1016/j.applthermaleng.2020.115791>
- R. Hölzl, in *Proc. of the ASME 2012 Pressure Vessels & Piping Conference 2012*, American Society of Mechanical Engineers, New York **2012**, 871–875. DOI: <https://doi.org/10.1115/PVP2012-78343>
- R. Hölzl, T. Hecht, P. Freko, in *Proc. of the ASME Pressure Vessels & Piping Division Conference 2014*, American Society of Mechanical Engineers, New York **2014**, V003T03A045. DOI: <https://doi.org/10.1115/PVP2014-28391>
- P. Freko, I. Thomas, R. Hoelzl, A. Lehmacher, A. Woitalka, in *Int. Heat Transfer Conf. 2014*, Begell House, Danbury, CT, **2014**, 3715–3725. DOI: <https://doi.org/10.1615/IHTC15.hex.009791>
- A. Hartog, *J. Lightwave Technol.* **1983**, *1* (3), 498–509.
- K. O. Hill, Y. Fujii, D. C. Johnson, B. S. Kawasaki, *Appl. Phys. Lett.* **1978**, *32* (10), 647–649.
- D. Yang, T. Liu, Z. Ding, Q. Han, K. Liu, J. Jiang, Q. Chen, B. Feng, *IEEE Photon. Technol. Lett.* **2014**, *26* (11), 1150–1153. DOI: <https://doi.org/10.1109/LPT.2014.2317702>
- H.-E. Joe, H. Yun, S.-H. Jo, M. B. Jun, B.-K. Min, *Int. J. of Precis. Eng. Manuf.-Green Technol.* **2018**, *5* (1), 173–191. DOI: <https://doi.org/10.1007/s40684-018-0017-6>
- A. K. Sang, M. E. Froggatt, D. K. Gifford, S. T. Kreger, B. D. Dickerson, *IEEE Sensors J.* **2008**, *8* (7), 1375–1380. DOI: <https://doi.org/10.1109/JSEN.2008.927247>
- C. Boyd, B. Dickerson, B. Fitzpatrick, in *Proc. of the Intelligent Ships Symposium*, **2011**, IX, 25–26.
- A. Ukil, H. Braendle, P. Krippner, *IEEE Sensors J.* **2012**, *12* (5), 885–892. DOI: <https://doi.org/10.1109/JSEN.2011.2162060>
- A. Barrias, J. R. Casas, S. Villalba, *Sensors (Basel, Switzerland)* **2016**, *16* (5), 748. DOI: <https://doi.org/10.3390/s16050748>
- R. Hoffmann, R. Flüggen, C. Richardt, J. Ferstl, C. Kerber, K. Braun, *WIT Trans. Eng. Sci.* **2016**, *106*, 185–195. DOI: <https://doi.org/10.2495/HT160181>